International Journal of Hydrogen Energy 140 (2025) 585–593

Contents lists available at ScienceDirect

International Journal of Hydrogen Energy

journal homepage: www.elsevier.com/locate/he

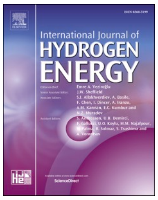

Fabrication of polyimide doped MOF/organosilica tubular membranes for H_2/CO_2 separation

Tong Wang, Shufeng Wu, Yuanyan Liu, Hong Qi *

College of Chemical Engineering, Nanjing Tech University, Nanjing, 211816, China

ARTICLE INFO

Handling Editor: Ramazan Solmaz

Keywords:
Polyimide
Organosilica
Hydrogen
Membranes
Doping

ABSTRACT

Organosilica membranes demonstrating robust hydrothermal stability show great potential for pre-combustion CO_2 capture, and the incorporation of ZIF-7 nanocrystals can effectively mitigate the trade-off effect typically associated with organosilica membranes. However, the phase transition of the ZIF-7 framework occurs when the solvent is removed. Polyimide (PI), a rigid polymer, was introduced after doping nanocrystals into 1, 2-bis(triethoxysilyl)ethane (BTESE). This approach effectively preserves the crystalline framework of ZIF-7 while maintaining high gas permeability and significantly enhancing both H_2/CO_2 and H_2/N_2 selectivity. Furthermore, it improves the overall hydrothermal stability of the hybrid membrane. When measured 200 °C, the PZB-5 wt % membrane demonstrated a hydrogen permeance of 2.34×10^{-6} mol m^{-2} s^{-1} Pa^{-1}, with impressive selectivity ratios of 5.54 for H_2/CO_2 and 25.2 for H_2/N_2. The findings indicate that the stability of nanoparticle-doped BTESE-derived membranes is markedly improved by the inclusion of rigid polymers.

1. Introduction

Hydrogen energy is an important alternative that can alleviate the greenhouse effect exacerbated by the use of fossil fuels [1]. At present, the principal methods for hydrogen production are methane steam reforming and the water-gas shift reaction. These methods can not only yield high concentrations of hydrogen, but also allow for the capture of carbon dioxide prior to combustion. During the natural gas reforming process, the mixed gas is mainly composed of H_2 and CO_2 (the typical reaction is: $CO + H_2O \rightarrow CO_2 + H_2$) [2]. Common H_2 purification techniques include pressure swing adsorption separation, cryogenic methods, and membrane technology. Of these ways, membrane separation technology has drawn significant focus in recent years because of its simple process, environmental compatibility, and energy efficiency. Hydrogen purification membranes can be classified into three categories based on their materials: organic polymer membranes, inorganic membranes, and mixed matrix membranes (MMMs). The SiO_2 membrane is the most commonly used inorganic membrane in gas separation due to its excellent thermochemical stability and high mechanical strength. However, its structure could not be applied for H_2/CO_2 separation in water-gas shift reactions [3,4]. Currently, a highly effective strategy for enhancing the MMMs performance, have already become a research focus, involves the uniform dispersion of organic or inorganic nanoparticles within a polymer matrix [5].

To improve the ability of SiO_2 membranes to withstand water vapor attack, organosilica membranes are prepared by introducing organic groups, such as BTESE [6], methyltriethoxysilane (MTES) [7], bis(triethoxysilyl)methane (BTESM) [8]. Kanezashi et al. [6] first proposed the application of BTESE in gas separation. Their results showed that the H_2 permeability reached 10^{-6} mol m^{-2} s^{-1} Pa^{-1}. The BTESE membrane demonstrates exceptional hydrothermal stability, attributed to the incorporation of Si–CH_2–CH_2–Si linkages within its structure. However, the membrane has poor H_2/CO_2 selectivity because of the presence of vinyl groups. Researchers doped metal (palladium, niobium, or metal-organic frameworks) into the network structure of organosilica membranes. This process allowed for the regulation of the network structure and alteration of the affinity between permeable gases and the membranes. Qi et al. [9,10] fabricated Nb-doped organosilica membranes and study the implication of Nb-doping amount and calcination temperature on the structure and gas performance of Nb-BTESE membranes. They noticed that Nb forms Nb–O–Si covalent bonds with BTESE networks, and the membrane structure tends to be dense with the increase of Nb content. Zhang et al. [11] combined ZIF-8 with polyimide to prepare MMMs for the separation of C_3H_6/C_3H_8. Their results showed that there was good adhesion between ZIF-8 and polyimide due to the hydrophobicity of the nanoparticles. The experimental results

---

* Corresponding author.
E-mail address: hqi@njtech.edu.cn (H. Qi).

https://doi.org/10.1016/j.ijhydene.2025.05.317
Received 3 March 2025; Received in revised form 2 May 2025; Accepted 22 May 2025

demonstrated that the ZIF-8/6FDA-DAM composite membrane exhibited a remarkable C_3H_6 permeability of 56.2 Barrer coupled with an exceptional C_3H_6/C_3H_8 ideal selectivity of 31.0. The MMM containing 48.0 wt% ZIF-8 nanoparticles demonstrated significantly enhanced performance, showing a 258 % rise in permeability and a 150 % enhancement in selectivity, compared to the 6FDA-DAM polymer membrane. Ma et al. [12] prepared MMMs by flat-scraping, in which ZIF-7 flakes were dispersed in a PI solution and coated on a glass plate. Because ZIF-7 sheets were encapsulated with polymer, and the main permeation channel was ZIF-7 with diameter of approximately 0.21 nm. The MMMs had an H_2 permeance of 3.5×10^{-7} mol m^{-2} $s^{-1}\cdot Pa^{-1}$, together with the ideal separation factors of H_2 with regard to CO_2, CH_4, and C_3H_8 were 104.8, 135.3 and 451.5, respectively, which were much higher than the corresponding Knudsen coefficients (4.7, 2.8, and 4.7). Metal-organic frameworks (MOFs) represent a class of highly porous materials characterized by uniform pore size combined with metal and organic ligands, which have the characteristics of great surface area, diverse structure [13,14]. Zeolite imidazolate framework (ZIF), as MOF derivatives, possess zeolite-like structures, and ZIF-7 is widely recognized as one of the most prominent ZIF materials, primarily due to its unique combination of properties, including the gate-opening effect, robust thermal stability, natural hydrophobicity, and exceptional hydrogen selectivity over other light gas molecules [14–17].

However, during the solvent removal or under high temperature and high pressure conditions, ZIF-7 will undergo three different crystalline phase transitions as follows: initially from a neat macro-porous structure (ZIF-7-I) to a skewed narrow structure (ZIF-7-II), and finally a layered non-porous structure (ZIF-7-III) when the guest molecules are removed [18,19]. These phase transitions can cause deformation of the mixed matrix membrane and clogging of pores, affecting the gas permeability. To solve this problem, Yang et al. [20] selected the glassy polymer 2, 2'-(poxydiphenyl)-5,5′-bibenzimidazole (OPBI) as the substrate to regulate the phase transition of ZIF-7. OPBI has a rigid polymer backbone and high chain stacking. Their study found that the ZIF-7-II/OPBI MMM had a H_2/CO_2 permselectivity of 27.1, which was higher than that of the MMM with ZIF-7-I. This indicates that the ZIF-7-II/OPBI MMM has better size-sieving functionality for H_2/CO_2 separation. Pan et al. [21] selected several polymers, such as polysulfone (PSF), Pebax®1657, polyimide, polydimethylsiloxane (PDMS), to explore their fixing effects on the phase transition of ZIF-7. Results showed that ZIF-7 showed phase II in PDMS polymers and phase I in other polymers, indicating that polymers with rigid segments can prevent the phase shift of ZIF-7 flexible frameworks. Therefore, inspired by the above-mentioned study, polymers with rigid characteristics were selected to maintain the skeleton structure of nanoparticles. Of the various polymers, polyimide based on 6FDA monomers are capable of both high gas permeability and selectivity. This is due to the bulky –$C(CF_3)_2$- group that hinders the mobility of the intrinsic segment, disrupting the interchain build-up and stiffening the backbone. In addition, polyimide based on 6FDA monomers exhibit many other properties required for membrane preparation, most notably its superior mechanical strength, excellent chemical and thermal resistance [22–26]. Dogan et al. [27] prepared polyimide with 6FDA monomer, and found that 6FDA-DAM was closer to the functionalized MOF surface. There was even a small overlap area between the MOF surface and the polymer, suggesting a robust interfacial interaction between the polymer and the MOF. As a result, many 6FDA polyimide materials have been used to make high-performance membranes [28].

In this paper, polyimide (PI), a rigid polymer, is introduced after doping nanoparticles into the organosilicon network structure. This could not only maintain the crystalline architecture of ZIF-7 nanoparticles, maintain the permeance of the hybrid membrane, but also enhance the membrane gas permselectivity and hydrothermal stability simultaneously. The hybrid membranes were synthesized through a dip-coating process, wherein the hybrid sols were uniformly deposited onto porous tubular γ-Al_2O_3/α-Al_2O_3 composite supports, subsequently subjected to thermal treatment at elevated temperatures under a controlled nitrogen atmosphere. The successful incorporation of polyimide (PI) into the MOF/BTESE hybrid networks was systematically verified through comprehensive characterization techniques, including FT-IR spectroscopy, X-ray diffraction, Scanning Electron Microscopy/Energy Dispersive Spectroscopy (SEM/EDS), and Transmission Electron Microscopy (TEM). Furthermore, the correlation between PI doping concentration and the resultant gas performance of the PI-MOF/organosilica composite membranes was thoroughly researched, revealing a notable enhancement in both permeability and permselectivity.

2. Experimental

2.1. Synthesis of ZIF-7 nanocrystals

ZIF-7 was prepared following the methodology reported [15,29]. BzIM (0.5907 g) was added and dissolved in MeOH (50 mL) and zinc nitrate hexahydrate (1.4875 g) was dissolved in 50 mL of DMF. The Zn^{2+} solution was joined to the BzIM solution and stirred at room temperature for 6 h. The products were collected and processed by centrifugation in a centrifuge (Xiangyi H1850, 8000 r/min) for 5 min, and subjected to three additional MeOH washes. The synthesized ZIF-7 were subsequently subjected to drying at 60 °C for 12 h to ensure complete solvent removal.

2.2. Preparation of PI

The PI was fabricated via direct polymerization [30]. 6.364 g 6FDA and 2.152 g DAM were added and dissolved in 30 mL NMP. The mixture was stirred in ice bath for approximately 24 h. Next, 6 mL of NMP and 2 mL of trimethylamine, together with 5.4 mL of acetic anhydride were added into the mixture. After chemical imidization, the polyimide solution was rinsed with MeOH for three times. Finally, the polymer fibers were heat treated at 200 °C for 24 h.

2.3. Preparation of PI-ZIF-7/BTESE hybrid sols

The procedure for preparing the PI-MOF/organosilicon hybrid sol is illustrated in Fig. 1. The hybrid sols were prepared by first dissolving ZIF-7 powders (0.1279 g) and PI in DMF (42 mL) under 15 min ultrasonication. To the mixture, 8 mL of BTESE sols were subsequently added, followed by another 15 min ultrasonication. The resulting PI-ZIF-7/BTESE sols were finally modified with 1 mL HCl solution. The obtained sols, powders, and hybrid membranes were assigned the designation PZB-*x* (*x* = 0 wt %, 2 wt %, 5 wt %, 7 wt % and 10 wt %) based on the mass ratios of PI to nanoparticles, while the molar ratio of

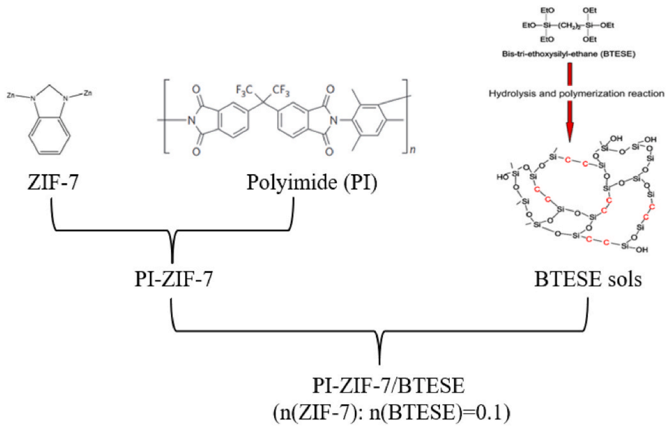

Fig. 1. Schematic illustration of the preparation of PI-ZIF-7/BTESE sols.

nanoparticles to organosilica was maintained at 0.1. Detailed experimental procedures regarding the preparation of BTESE sols, PI-ZIF-7/BTESE membrane fabrication, are provided in the supporting information.

2.4. Gas permeation measurements

The gas (He, H_2, CO_2, N_2, CH_4, and SF_6) permeability of PZB-x hybrid membranes was measured at 200 °C with a feed pressure of 3 bar on a home-made equipment reported in previous research work [31]. The hydrothermal stability of the membranes was evaluated by comparing their gas permeability before and after treatment with different saturated water vapor (0 kPa, 20 kPa, 40 kPa, 60 kPa, 80 kPa, 100 kPa. The tested membrane's gas performance was measured when dry). This gas transport properties were calculated with equation (1):

$$P_i = \frac{F_i}{A \Delta P} \tag{1}$$

where P_i is the permeance of gas i ($mol \cdot m^{-2} \cdot s^{-1} \cdot Pa^{-1}$), F_i is the flux of the membrane ($mol \cdot s^{-1}$), A is the effective area of the ceramic membrane (m^2), ΔP is the transmembrane pressure (Pa).

The ideal gas separation factor (a) of membrane is calculated with the following equation (2):

$$a = \frac{P_i}{P_j} \tag{2}$$

where P_i and P_j are the permeance of gas i and j, respectively.

3. Results and discussion

3.1. Characterization of PI polymers

The thermal stability of PI was analyzed by differential scanning, as shown in Fig. 2(a). Under a nitrogen atmosphere, PI demonstrated exceptional thermal stability. However, its structure began to decompose and its weight began to decrease above 500 °C. Its glass transition temperature was 400 °C. FT-IR spectra of PI was displayed in Fig. 2(b). It can be seen that the symmetrical stretching vibration absorption peaks of C═O bonds were found around 1780 cm^{-1} and 1720 cm^{-1}. The expansion and contraction vibrational absorption peaks of the C–N bond on the imide ring can be observed around 1380 cm^{-1}. These peaks are characteristic of PI. There was no obvious carboxy hydroxyl vibration peak near 2900-3200 cm^{-1}, indicating that the characteristic peak of PAA disappeared and the degree of imidization was complete. At the same time, the deformation and expansion vibration peaks of C–F bond were observed near 1424 cm^{-1} and 1173 cm^{-1}, respectively, indicating that fluorine-containing groups were introduced into PI [32].

3.2. Chemical properties of sols and powders

Fig. 3(a) and (b) show optical photographs and colloidal dimension distributions of different doping amounts of PZB-x sols. It is evident that PZB-x sols are clear and transparent, without any precipitation. It can be seen in Fig. 3(b) that the sol particle size shows a broader distribution, and the BTESE sol demonstrates a well-controlled particle size distribution, with all particles measuring less than 10 nm in diameter [31]. ZIF-7 nanocrystals were incorporated into the BTESE network structure, which induces a noticeable enlargement in the average particle size of the BTESE sol (ZIF-7/BTESE sol size larger than 1 μm). Subsequently, PI doping is intertwined with the ZIF-7/BTESE network and tightly bound. The average particle size of PZB-x sols is about 1 μm, indicates that the doping amount of PI polymer did not significantly change the colloidal dimension distribution of ZIF-7/BTESE sol.

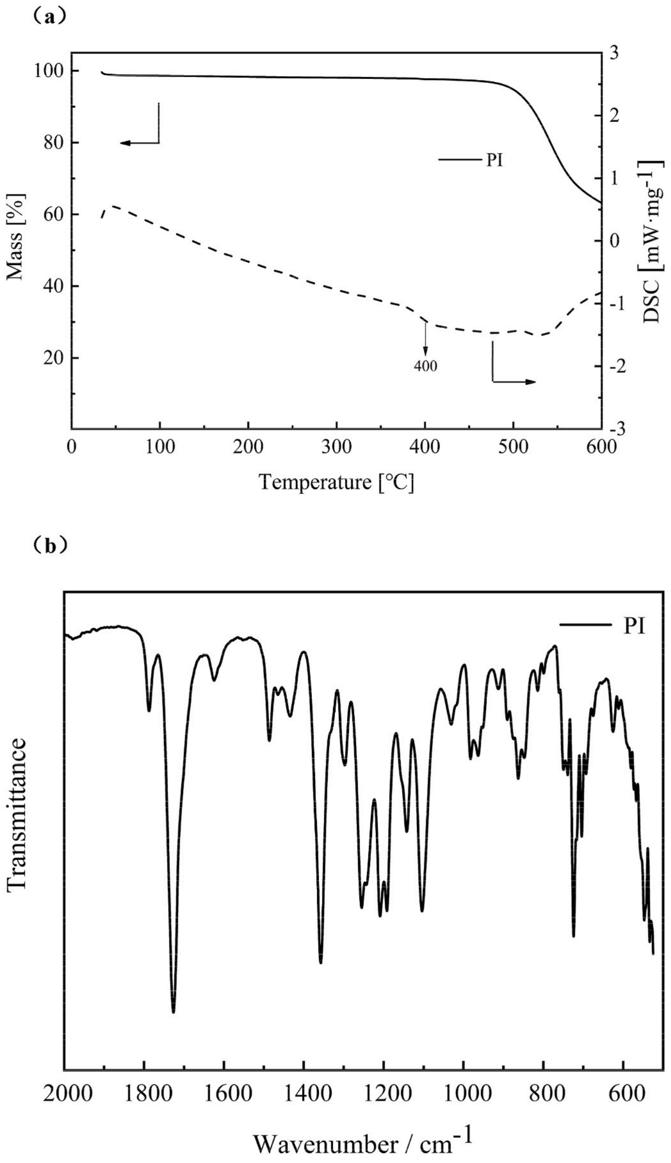

Fig. 2. TG-DSC (a) and FTIR (b) curves of PI polymer.

The BTESE membranes will undergo a calcination process at 400 °C in a nitrogen atmosphere during preparation. In this case, if structurally stable PZB membrane is to be fabricated, thermal stability represents a crucial parameter for both ZIF-7 nanocrystals and PI polymers, significantly influencing their potential applications. Fig. S1 presents the TGA curves of ZIF-7, BTESE, ZIF-7/BTESE and PI-ZIF-7/BTESE powders at 30–600 °C. ZIF-7, BTESE and PI (Fig. 2(a)) all have good thermal stability. The doping of ZIF-7 nanocrystals into the BTESE improved the degradation temperature. Upon incorporation of PI into the ZIF-7/BTESE network structure, the resulting PZB composite powders exhibited a marginal decrease in thermal stability compared to the pristine ZIF-7/BTESE system. At 400 °C, the mass loss of PZB powder (24 %) was greater than that of ZIF-7/BTESE powder (14 %), which may be due to the presence of nanoparticles that interferes with the polymer backbone and leads to a higher fractional free volume [33].

Fig. 4(a) shows XRD patterns of PZB-x powders. According to the literature, the XRD spectra of PI powder and BTESE powder exhibits a wide signal spanning the 2θ range of 5–40°, reflecting its non-crystalline structure with short-range ordering, which confirms its disordered nature [34,35]. The distinctive diffraction peaks corresponding to the crystalline structure of ZIF-7 in PZB powders are hardly observable, which may be due to the overlap with the diffraction peaks of PI and BTESE powders. Another contributing factor for this phenomenon may

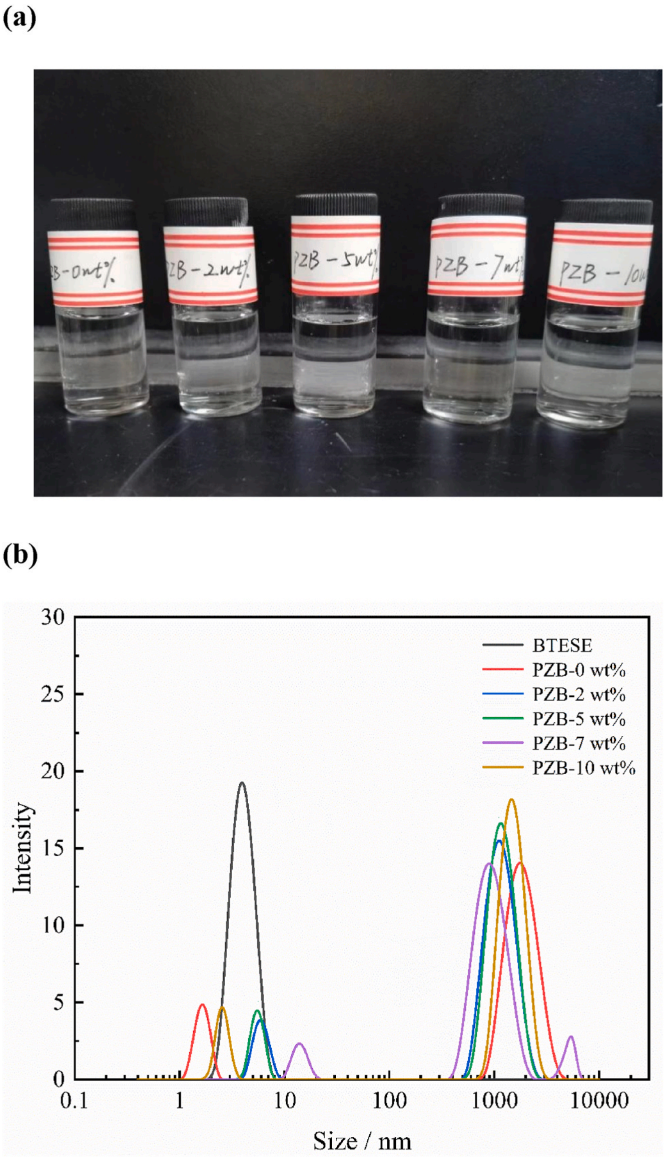

Fig. 3. (a) Optical photographs and (b) Size distribution of PZB-*x* sols.

result from the low ZIF-7 content in this recipe (n (ZIF-7): n (BTESE) = 0.1). The XRD pattern of the synthesized ZIF-7 nanoparticles shows excellent agreement with the standard ZIF-7 reference (see Fig. S2), with all characteristic peaks matching their corresponding crystal planes [29]. This confirms the successful preparation of phase-pure ZIF-7 nanoparticles. ~3450 $cm^{-1}$and ~1045 cm^{-1} correspond to the telescopic vibration of Si–OH and the asymmetric telescopic vibration of Si–O–Si in BTESE powder, respectively [36,37]. The emergence of new chemical bonds was evidenced by a distinct vibrational band at 1506 cm^{-1} and 743 cm^{-1}, which can be attributed to the vibrational modes of C═C and C–H bonds within the benzimidazolate ligands of the ZIF-7 framework [38]. The characteristic peaks of PI polymer are shown in Fig. 2(b), and as can also be seen from the infrared spectrum of the PZB-*x* powders, all the characteristic imide bands are retained with the addition of PI polymer. As the doping content of fluorinated dianhydride polymer increased, the strength of the absorption peaks for the symmetrical stretching vibrations of the C═O bond (corresponding to 1720 cm^{-1}) also increased.

Fig. 5(a) demonstrates a crack-free membrane surface, confirming the successful preparation of a continuous membrane. The randomly dispersed fibrous aggregates observed on the membrane surface may originate from either residual pollutant during sample preparation. As shown in Fig. 5(b), the membrane exhibits uniform thickness with smooth cross-sectional morphology. Fig. S3(a) and (b) present the EDS elemental mapping of both surface and cross-section of the PZB-5 wt% membrane, which verifies the successful incorporation of Zn and F elements into the BTESE network. The relatively low mass percentage of F element correlates with the low doping concentration of PI in the hybrid membrane.

Fig. 6(a) presents the TEM image of PZB-0 wt% powder, where the dark spots with distinct lattice fringes (see Fig. S4(a)) correspond to ZIF-7 nanoparticles [38]. Their uniform distribution throughout the network confirms the successful incorporation of ZIF-7 crystals into the BTESE matrix. Fig. 6(b) displays the TEM results for PZB-5 wt% powder. The introduced PI polymer effectively encapsulates and immobilizes the ZIF-7 crystals, stabilizing their flexible framework while maintaining the structural integrity of ZIF-7 nanoparticles, as further evidenced by the preserved crystallinity shown in Fig. S4(b). The less distinct appearance of the black spots in Fig. 6(b) compared to (a) may be attributed to PI encapsulating the ZIF-7 nanoparticles.

Fig. 7 presents XRD patterns of PZB-*x* powders after saturated water vapor treated at 100 kPa for 48 h. Compared with Fig. 4(a), it is evident that there is no discernible difference in the PZB-*x* powders before and after hydrothermal treatment, indicating that the structure of the PZB powders is highly resistant to water vapor. This is due possibly to the

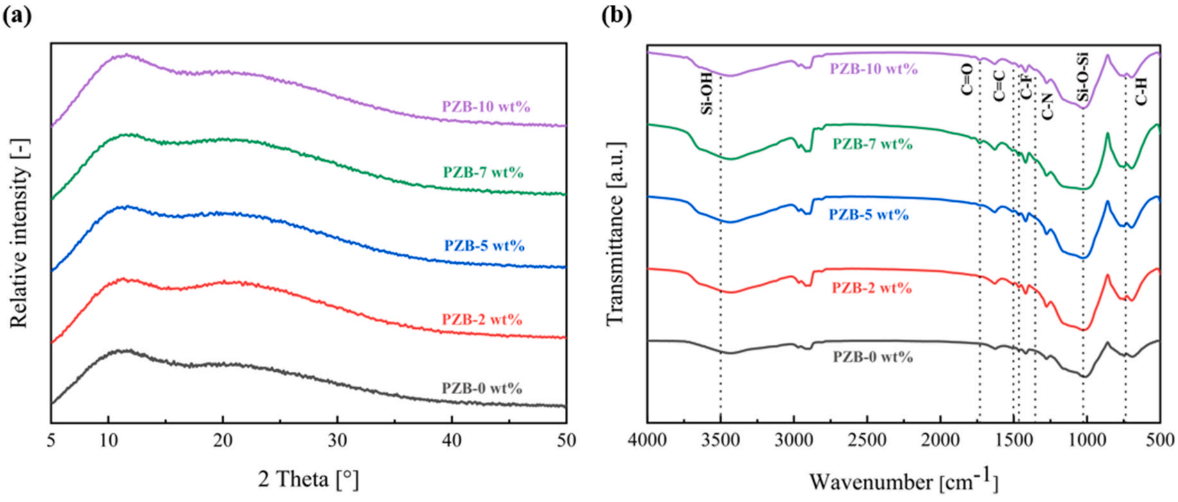

Fig. 4. (a) XRD patterns and (b) FTIR spectra of PZB-*x* powders.

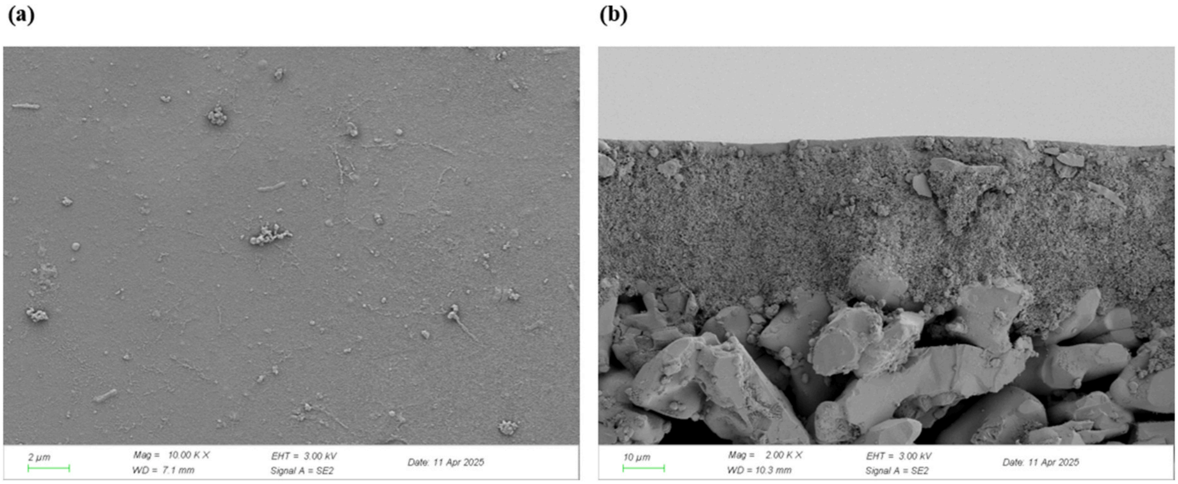

Fig. 5. (a) Surface and (b) cross-sectional SEM images of PZB-5 wt% membrane.

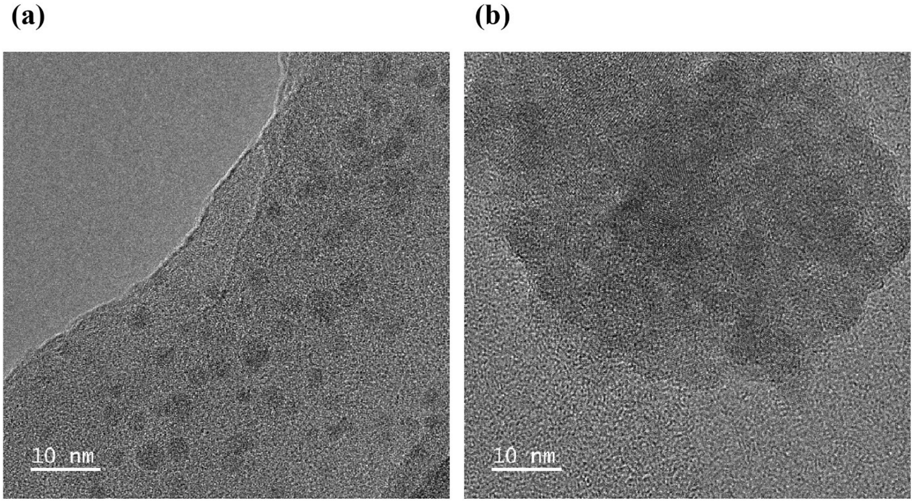

Fig. 6. TEM images of (a) PZB-0 wt% powder and (b) PZB-5 wt% powder.

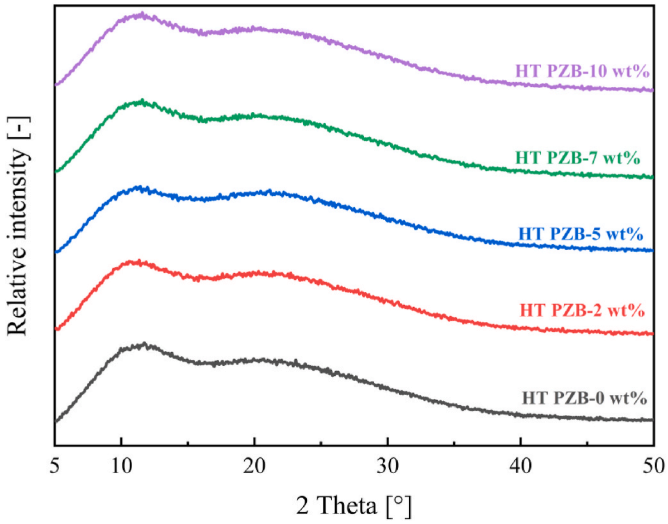

Fig. 7. XRD patterns of PZB-*x* powders after hydrothermal treatment.

strong hydrophobicity of the –C$(CF_3)_2$- group contained in the PI polymer and the vinyl group in BTESE. On the other hand, ZIF-7 nanocrystals with coordination bonds formed by metal and organic ligands also have some corrosion resistance towards water vapor.

3.3. Permeation characteristics of hybrid membranes for gas separation

Fig. 8 shows the permeability of PZB-*x* membranes with different PI contents with regard to six different gases and the permselectivity for H_2/CO_2, H_2/N_2 measured at 200 °C. The gas separation characteristics of ZIF-7/BTESE membranes were thoroughly examined following the introduction of PI polymer, with particular attention to permeability and selectivity parameters. With the increasing of PI doping, the gas permeability of PZB membranes decreased a little but still maintained a high H_2 permeability ($\sim 10^{-6}$ mol m^{-2} s^{-1}·Pa^{-1}). On the one hand, the regular pore structure of ZIF-7 provides a fast channel for the permeability of H_2 inside the membrane, and the incorporation of ZIF-7 nanoparticles significantly enhances the membrane's free volume characteristics while creating additional sub-nanometer-scale transport channels, thereby facilitating more efficient gas permeation through the composite membrane structure. On the other hand, after incorporating PI polymer into MOF/organosilica membranes, a double network structure is formed with BTESE, forming a non-selective gap and increasing the gas delivery channel.

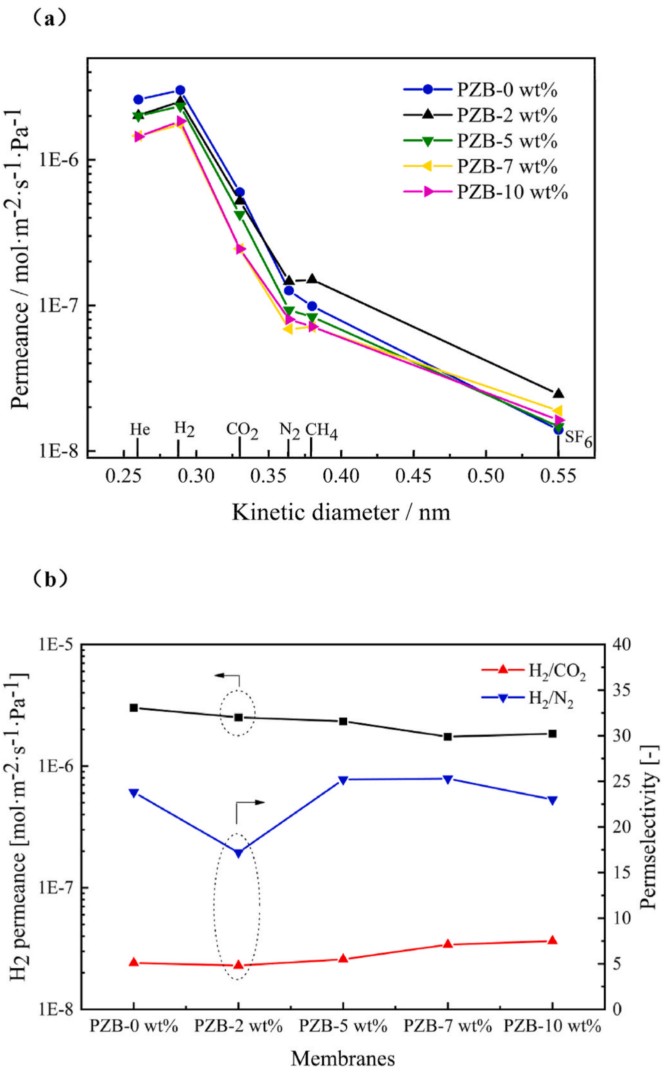

Fig. 8. (a) Six gases permeability and (b) H_2/CO_2, H_2/N_2 permselectivity of PZB-*x* hybrid membranes tested at 200 °C.

From Fig. 8(b), the permselectivity of PZB membranes is also incrementally rising, and CO_2 molecules ($d_{CO2} = 0.33$ nm $> d_{ZIF\text{-}7} = 0.30$ nm) cannot be diffused in the pores of ZIF-7, that is, the addition of ZIF-7 lengthens the permeability path of CO_2 and increases permeability resistance of CO_2 inside the hybrid membrane. When the amount of PI doping increases, the non-selective gap between ZIF-7 and the dual network structure decreases, which also increases the osmotic resistance of CO_2 in the hybrid membrane. Although the increase of the free volume of the membrane can also improve the permeability of CO_2, the restriction of CO_2 by the pore size and non-selective gap of ZIF-7 are much greater than the effect of the increase of free volume on the CO_2 molecules. Meanwhile, the imide group of the PI polymer forms more hydrogen bonds with BTESE, which results in a stronger interaction between the networks. However, excessive doping can cause the PI polymer to wind and obstruct the pores, leading to decreased gas permeability. Thus, a moderate amount of PI doping can make the PZB hybrid membranes have a high H_2 permeability and enhance a certain H_2/CO_2 selectivity. At 200 °C, the PZB-5 wt % hybrid membrane shows an H_2 permeance of 2.34×10^{-6} mol m^{-2} s^{-1} Pa^{-1}, H_2/CO_2 and H_2/N_2 permselectivity of 5.54 and 25.2, respectively.

To elucidate the mass transport mechanisms of six distinct gases through the PZB-*x* membrane series, a systematic investigation was conducted to examine the temperature-dependent gas permeability behavior of the hybrid membranes. The gas activation energy of the PZB-*x* membranes can be calculated according to the following equation [39]:

$$P = P_0 \exp\left(\frac{-\Delta E}{RT}\right) \tag{3}$$

$$lnP = -\frac{\Delta E}{RT} + ln\,P_0 \tag{4}$$

The gas permeance (*P*), expressed in units of mol·m^{-2} s^{-1} Pa^{-1}, can be characterized by the following parameters: P_0 represents the temperature-independent pre-exponential factor, *R* denotes the gas constant (kJ·mol^{-1} K^{-1}), *T* corresponds to the absolute temperature during permeation measured in Kelvin (K), and *ΔE* signifies the apparent activation energy of permeation, quantified in kJ·mol^{-1}.

Fig. 9 shows the single gas permeance of the PZB-5 wt % membrane is plotted against temperature, revealing its temperature dependence. The gas permeability of He and H_2 increases with the rise of the test temperature (from 50 °C to 200 °C). Fig. 9(b) shows the result of a linear fit from ln (F) and 1000/RT, and the slope of the fitted straight line is -ΔE [kJ·mol^{-1}] (Eq. (4)). $\Delta E>0$ reveals that gas permeation across the membrane is governed by an activated diffusion mechanism, whereas $\Delta E<0$ implies the predominance of surface diffusion mechanism in the transport process [40]. Therefore, the linear regression analysis reveals distinct temperature dependence patterns: the fitted curves for He, H_2, N_2, and CH_4 demonstrate negative slopes, whereas CO_2 and SF_6 exhibit positive slopes in their respective temperature-permeability relationships. This observation indicates that He, H_2, N_2, and CH_4 exhibit positive activation energies, showing that their transport across the membrane occurs via an activated diffusion process, where molecular permeation requires overcoming an energy barrier. Furthermore, the negative activation energies of CO_2 and SF_6 demonstrate that the same mechanism is surface diffusion. The higher the value of activation energy, the greater the resistance that the gas needs to overcome through the membrane, and the denser of the membrane structure.

The pore size distribution of PZB-*x* hybrid membranes was quantitatively characterized using the Normalized-Knudsen Permeance (NKP) method, as illustrated in Fig. S5. The NKP values were calculated according to Eq (5), which describes the relationship between gas permeance and membrane pore dimensions [41,42].:

$$f_{NKP} = \frac{P_i}{P_{He}}\sqrt{\frac{M_i}{M_{He}}} = \frac{(d_P - d_{k,i})^3}{(d_P - d_{k,He})^3} \tag{5}$$

where P_i, P_{He} are the true permeances of gas *i* and *He* (mol·m^{-2}·s^{-1}·Pa^{-1}), M_i and M_{He} are the molecular weight of gas *i* and *He*, d_p is the NKP pore size (Å), $d_{k,i}$ and $d_{k,\ He}$ are the dynamic diameters of gas *i* and *He* (Å), respectively.

Fig. S5 shows the molecular size-dependent NKP characteristics of PZB-*x* hybrid membranes. Except for the ZIF-7/BTESE membrane, according to the fitting curve, the calculated pore sizes of the hybrid membranes first increased, then decreased and increased finally, the minimum membrane pore size was 0.470 nm (PZB-5 wt % membrane). This may be due to the sudden increase in membrane pore size after the introduction of PI. However, with an increase of the doping amount, the interaction between the polymer and the ZIF-7/BTESE network strengthened, resulting in a tighter bond. This caused the membrane pore size to decrease initially and then increase. By modulating the doping amount of PI, the pore diameter of the PZB-*x* hybrid membranes can be finely tuned, which directly impacts their separation performance. Fig. S6 shows the H_2 permeability and H_2/CO_2 permselectivity of the PZB-*x* membranes tested at 200 °C as a function of time. After 120 h of gas permeability test, the PZB-5 wt % hybrid membrane showed an H_2 permeability of 2×10^{-7} mol m^{-2} s^{-1}·Pa^{-1}, and H_2/CO_2 permselectivity of 5.56. It can be seen form Fig. S6 that PZB-*x* hybrid membrane showed remarkable stability over prolonged use.

Because the pre-combustion capture process involves a shift reaction,

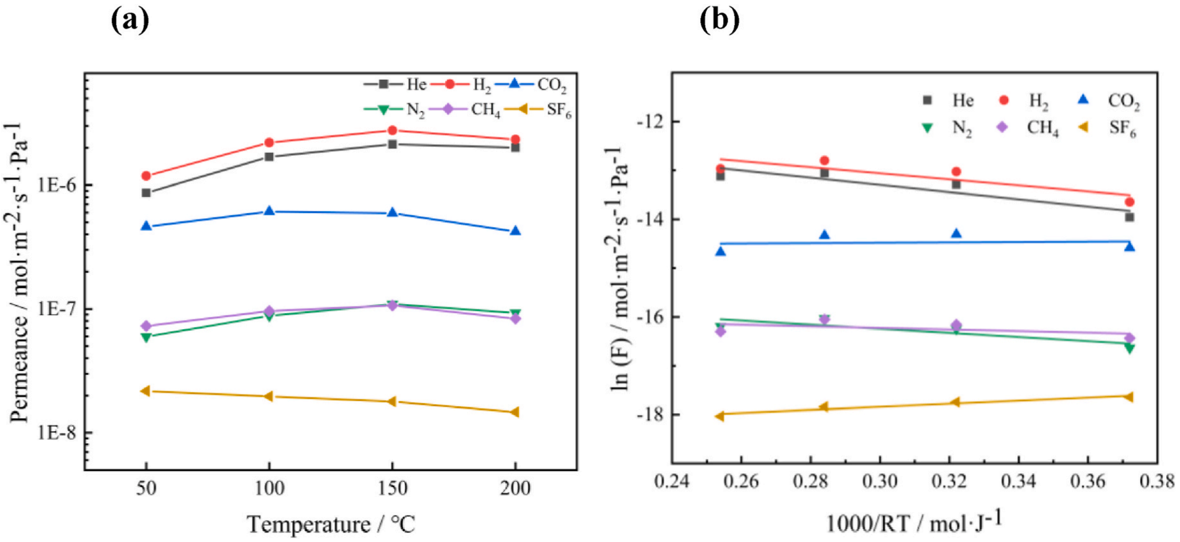

Fig. 9. (a) Temperature-dependent gas transport properties (b) temperature dependance of gas calculated by Arrhenius equation with regard to PZB-5 wt % membrane.

which is conducted under high reaction pressure and water vapor [43], the hydrothermal stability of hybrid membranes also needs to be investigated. The ZIF-7 nanocrystals have a flexible framework, and thus there are solvents within the structure. After complete removal of the solvents, the metal-organic framework will undergo a phase transition from phase I to phase II, eventually resulting in a non-porous material [18,19]. But, the presence of the rigid –C(CF_3)$_2$- group in the PI structure can fix the ZIF-7-I structure and limit the migration of the structure (Fig. 6(b)). Fig. 10 presents the gas permeability of H_2, CO_2 and N_2 and the permselectivity of H_2/CO_2 and H_2/N_2 of PZB-5 wt % hybrid membrane after treated with different saturated water vapors. As can be seen from the figure, there is a decrease of the H_2 permeability and H_2/CO_2 and H_2/N_2 permselectivity of the PZB-5 wt % hybrid membrane treated with 100 kPa saturated water vapor. The results showed the H_2 permeability was 5.98×10^{-7} mol m^{-2} s^{-1}·Pa^{-1} and the permselectivity of H_2/CO_2 was 4.61. The reason for this may be that the structure of polymer PI begins to change from rigid to flexible at a calcination temperature of 400 °C, leading to an inherent buildup of the main chain. Coupled with prolonged erosion by water vapor, the polymer may have low swelling, which destroys the membrane structure. Moreover, the competitive adsorption of water molecules on the polar imidazole ring, which leads to a lower permeation flux and a narrower effective pathway for CO_2, thus increasing the diffusion resistance of the gases. However, this factor has a minor influence because the gas performance data were measured under dry conditions. As shown in Fig. S7, the gas permeance of the PZB-5 wt% hybrid membrane decreased after 20 kPa hydrothermal treatment, likely due to hydrolysis of Si–O–Si bonds in the membrane. This process generates mobile Si–OH groups (evidenced by the increased ~3450 cm^{-1} Si–OH peak in Fig. S7), which may block the transport channels. It is also possible that the structure of the separating layer of the membrane tube was damaged because of the same membrane tube, which was subjected to several pressurization processes and hydrothermal stability operation experiments.

Table 1 shows a comparison of the H_2/CO_2 separation performance of hybrid materials with membranes reported in the literature, including MOF-doped mixed matrix membranes [12,20,44–47] and GO-based membranes [48]. Most of the MMMs studied in the literature reported low H_2 permeability. This is due to poor adhesion between the fillers and the substrate on the one hand. On the other hand, experiments reported in the literature are based on sheet substrates, resulting in low gas permeability. In our experiment, the tubular membrane was fabricated. The experimental results demonstrate that the PI-ZIF-7/BTESE hybrid

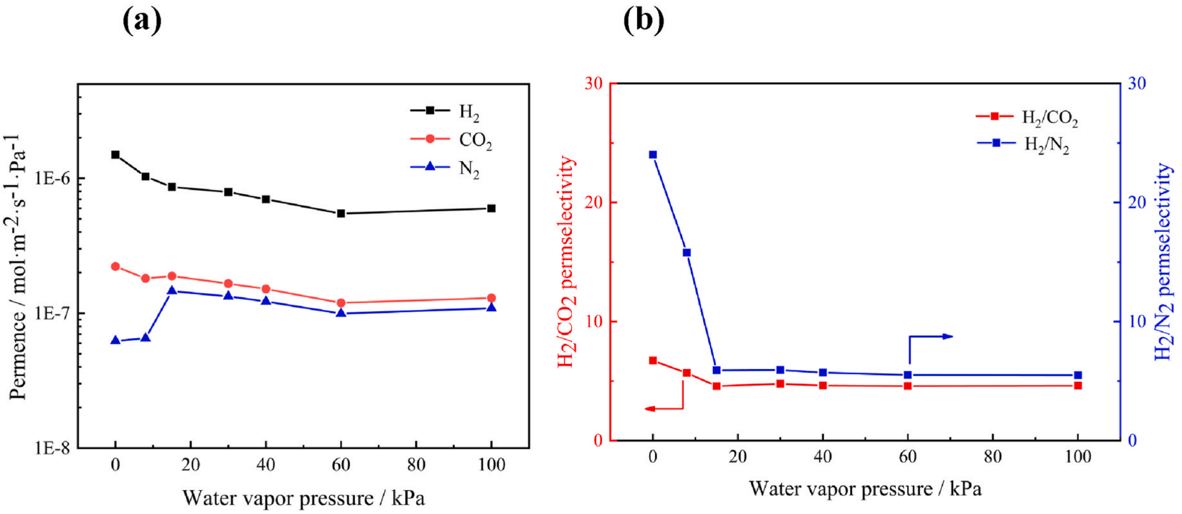

Fig. 10. (a) gas permeability and (b) H_2/CO_2 and H_2/N_2 separation performance of PZB-5 wt % hybrid membrane after hydrothermal treatment.

Table 1
H_2 permeability and H_2/CO_2 separation performance of membranes.

Membranes	Types	Separation system	Test conditions	Permeance (mol·m^{-2}·s^{-1}·Pa^{-1})	Permselectivity (−)	References
ZIF-7/PI	Plate	H_2/CO_2	2 bar, 100 °C	3.5×10^{-7} (H_2)	104.8	[12]
ZIF-7/OPBI	Plate	H_2/CO_2	4 bar, 25 °C	3.7×10^{-9} (H_2)	27.1	[20]
ZIF-7/PBI	Plate	H_2/CO_2	3.5 bar, 35 °C	3.7×10^{-9} (H_2)	14.9	[44]
ZIF-7/6FDA-DAM	Plate	H_2/CO_2	1 bar, 25 °C	1.3×10^{-7} (H_2)	4.35	[45]
PDA/ZIF-7/PSF	Plate	H_2/CO_2	4 bar, 30 °C	5.9×10^{-9} (H_2)	9.3	[46]
PSM-nZIF-7/PEI	Plate	H_2/CO_2	2.03 bar, 35 °C	2.9×10^{-9}(H_2)	8.2	[47]
r-GO/BTESE	Tube	H_2/CO_2	2 bar, 150 °C	2.5×10^{-7} (H_2)	4.1	[48]
APTES/BTESE	Tube	H_2/CO_2	1 bar, 200 °C	3.1×10^{-7} (H_2)	10	[49]
PI-ZIF-7/BTESE	Tube	H_2/CO_2	3 bar, 200 °C	2.3×10^{-6} (H_2)	5.5	This work

membranes exhibit exceptional H_2 permeance, with H_2/CO_2 permselectivity significantly surpassing the 2008 Robeson upper bound (4.8, as shown in Fig. S8) [31], indicating their great potential for practical hydrogen purification applications.

4. Conclusions

In summary, PI-ZIF-7/BTESE sols were successfully prepared, suitable for coating on a tubular γ-alumina support developed internally. The XRD, FTIR, SEM/EDS and TEM characterizations confirmed that polymers had been incorporated into MOF/organosilica structure. A comprehensive investigation was conducted to examine the influence of PI integration on both the separation efficiency and underlying transport phenomena in PZB-*x* composite membrane systems. Results showed that PI doping could maintain the high H_2 permeability of PZB membranes with improved the H_2/CO_2 permselectivity.

For the PI-ZIF-7/BTESE membrane, the rigid $–C(CF_3)_2-$ group in the PI polymer can fix the ZIF-7-I structure and limit the migration of the structure. Doping PI polymer can reduce the number of macropores inside ZIF-7/BTESE membranes, enhance the affinity between ZIF-7 nanocrystals and BTESE network, and therefore improve the stability of ZIF-7/BTESE. With the increase of PI doping amount, the interaction strengthened between the imide group and BTESE, making possible better separation performance of the hybrid membranes. At the test temperature of 200 °C, the H_2 permeability of PZB-5 wt % hybrid membrane was 2.34×10^{-6} mol m^{-2} s^{-1}·Pa^{-1}, and the selectivity of H_2/CO_2 and H_2/N_2 was 5.54 and 25.2, respectively. The experimental data from both the 120h durability assessment and hydrothermal stability evaluation consistently demonstrated that the PZB-5 wt % composite membrane maintained superior structural integrity under testing conditions.

CRediT authorship contribution statement

Tong Wang: Writing – review & editing, Writing – original draft. **Shufeng Wu:** Writing – original draft, Formal analysis, Data curation. **Yuanyan Liu:** Data curation. **Hong Qi:** Data curation.

Declaration of competing interest

The authors declare that they have no known competing financial interests or personal relationships that could have appeared to influence the work reported in this paper.

Acknowledgments

This work is supported by the National Natural Science Foundation of China (21490581), China Petroleum & Chemical Corporation (317008–6).

Appendix A. Supplementary data

Supplementary data to this article can be found online at https://doi.org/10.1016/j.ijhydene.2025.05.317.

References

[1] Xu J, Yang D, Zhang H, Guan M, Li Q, Cai M, et al. Selectivity enhancement by the presence of HOF plus CNT composite membranes investigated by non-equilibrium molecular dynamics. Sep Purif Technol 2024;330:125472. https://doi.org/10.1016/j.seppur.2023.125472.

[2] Li X, Singh RP, Dudeck KW, Berchtold KA, Benicewicz BC. Influence of polybenzimidazole main chain structure on H_2/CO_2 separation at elevated temperatures. J Membr Sci 2014;461:59–68. https://doi.org/10.1016/j.memsci.2014.03.008.

[3] Li H, Pieterse JAZ, Dijkstra JW, Boon J, van den Brink RW, Jansen D. Bench-scale WGS membrane reactor for CO_2 capture with co-production of H_2. Int J Hydrog Energy 2012;37:4139–43. https://doi.org/10.1016/j.ijhydene.2011.11.135.

[4] Duke MC, da Costa JCD, Do DD, Gray PG, Lu GQ. Hydrothermally robust molecular sieve silica for wet gas separation. Adv Funct Mater 2006;16:1215–20. https://doi.org/10.1002/adfm.200500456.

[5] Ren X, Kanezashi M, Nagasawa H, Xu R, Zhong J, Tsuru T. Ceramic-supported polyhedral oligomeric silsesquioxane-organosilica nanocomposite membrane for efficient gas separation. Ind Eng Chem Res 2019;58:21708–16. https://doi.org/10.1021/acs.iecr.9b05251.

[6] Kanezashi M, Yada K, Yoshioka T, Tsuru T. Design of silica networks for development of highly permeable hydrogen separation membranes with hydrothermal stability. J Am Chem Soc 2009;131. https://doi.org/10.1021/ja806762q. 414-+.

[7] Castricum HL, Sah A, Kreiter R, Blank DHA, Vente JF, ten Elshof JE. Hydrothermally stable molecular separation membranes from organically linked silica. J Mater Chem 2008;18:2150–8. https://doi.org/10.1039/b801972j.

[8] Kanezashi M, Kawano M, Yoshioka T, Tsuru T. Organic-inorganic hybrid silica membranes with controlled silica network size for propylene/propane separation. Ind Eng Chem Res 2012;51:944–53. https://doi.org/10.1021/ie201606k.

[9] Qi H, Chen H, Li L, Zhu G, Xu N. Effect of Nb content on hydrothermal stability of a novel ethylene-bridged silsesquioxane molecular sieving membrane for H_2/CO_2 separation. J Membr Sci 2012;421:190–200. https://doi.org/10.1016/j.memsci.2012.07.010.

[10] Qi H, Han J, Xu N. Effect of calcination temperature on carbon dioxide separation properties of a novel microporous hybrid silica membrane. J Membr Sci 2011;382:231–7. https://doi.org/10.1016/j.memsci.2011.08.013.

[11] Zhang C, Dai Y, Johnson JR, Karvan O, Koros WJ. High performance ZIF-8/6FDA-DAM mixed matrix membrane for propylene/propane separations. J Membr Sci 2012;389:34–42. https://doi.org/10.1016/j.memsci.2011.10.003.

[12] Ma X, Wu X, Caro J, Huang A. Polymer composite membrane with penetrating ZIF-7 sheets displays high hydrogen permselectivity. Angew Chem, Int Ed 2019;58:16156–60. https://doi.org/10.1002/anie.201911226.

[13] Li H, Eddaoudi M, O'Keeffe M, Yaghi OM. Design and synthesis of an exceptionally stable and highly porous metal-organic framework. Nature 1999;402:276–9. https://doi.org/10.1038/46248.

[14] Park KS, Ni Z, Cote AP, Choi JY, Huang R, Uribe-Romo FJ, et al. Exceptional chemical and thermal stability of zeolitic imidazolate frameworks. Proc Natl Acad Sci U S A 2006;103:10186–91. https://doi.org/10.1073/pnas.0602439103.

[15] Li Y-S, Liang F-Y, Bux H, Feldhoff A, Yang W-S, Caro J. Molecular sieve membrane: supported metal-organic framework with high hydrogen selectivity. Angew Chem, Int Ed 2010;49:548–51. https://doi.org/10.1002/anie.200905645.

[16] Aguado S, Bergeret G, Titus MP, Moizan V, Nieto-Draghi C, Bats N, et al. Guest-induced gate-opening of a zeolite imidazolate framework. New J Chem 2011;35:546–50. https://doi.org/10.1039/c0nj00836b.

[17] Xiang L, Sheng L, Wang C, Zhang L, Pan Y, Li Y. Amino-functionalized ZIF-7 nanocrystals: improved intrinsic separation ability and interfacial compatibility in mixed-matrix membranes for CO_2/CH_4 separation. Adv Mater 2017;29:1606999. https://doi.org/10.1002/adma.201606999.

[18] Zhao P, Lampronti GI, Lloyd GO, Wharmby MT, Facq S, Cheetham AK, et al. Phase transitions in zeolitic imidazolate framework 7: the importance of framework flexibility and guest-induced instability. Chem Mater 2014;26:1767–9. https://doi.org/10.1021/cm500407f.

[19] He M, Yao J, Li L, Wang K, Chen F, Wang H. Synthesis of zeolitic imidazolate framework-7 in a water/ethanol mixture and its ethanol-induced reversible phase

transition. Chempluschem 2013;78:1222–5. https://doi.org/10.1002/cplu.201300193.

[20] Yang S, Wang Y, Lu P, Jin H, Pan F, Shi Z, et al. Metal-organic frameworks corset with a thermosetting polymer for improved molecular-sieving property of mixed-matrix membranes. ACS Appl Mater Interfaces 2020;12:55308–15. https://doi.org/10.1021/acsami.0c17426.

[21] Xiang L, Liu D, Jin H, Xu L-W, Wang C, Xu S, et al. Locking of phase transition in MOF ZIF-7: improved selectivity in mixed-matrix membranes for O_2/N_2 separation. Mater Horiz 2020;7:223–8. https://doi.org/10.1039/c9mh00409b.

[22] Wang X, Ding Q, You R, Yu C, Li Y, Zhao J, et al. Mixed matrix membranes for C_2H_4/C_2H_6 separation using a phosphate anion-pillared microporous material. Ind Eng Chem Res 2023;62:18603–11. https://doi.org/10.1021/acs.iecr.3c02230.

[23] Qiu W, Xu L, Chen C-C, Paul DR, Koros WJ. Gas separation performance of 6FDA-based polyimides with different chemical structures. Polymer 2013;54:6226–35. https://doi.org/10.1016/j.polymer.2013.09.007.

[24] Liu Z, Liu Y, Qiu W, Koros WJ. Molecularly engineered 6FDA-based polyimide membranes for sour natural gas separation. Angew Chem, Int Ed 2020;59:14877–83. https://doi.org/10.1002/anie.202003910.

[25] Park J, Lee CO, Kim JW, Jo JH, Chi WS, Kim H. Poly(benzyl ether)-type additive to engineer glassy polyimide membranes for enhanced gas separations. Chem Commun 2022;58:4364–7. https://doi.org/10.1039/d1cc07017g.

[26] Park J, Lee CO, Kim KJ, Chi WS, Kim H. Tailoring 6FDA-based click cross-linked membranes: modular synthesis and tunable gas separation. Mol Syst Des Eng 2023;8:32–8. https://doi.org/10.1039/d2me00215a.

[27] Dogan EB, Maurin G, Ahunbay MG. Atomistic insight into the interfacial structuring of ZIF-67 MOF/polymer composites and their propylene-propane adsorption properties. J Phys Chem C 2023;127:20491–502. https://doi.org/10.1021/acs.jpcc.3c04377.

[28] Hua Y, Wang H, Li Q, Chen G, Liu G, Duan J, et al. Highly efficient CH_4 purification by LaBTB PCP-based mixed matrix membranes. J Mater Chem A 2018;6:599–606. https://doi.org/10.1039/c7ta07261a.

[29] He D, Zhang H, Ren Y, Qi H. Fabrication of a novel microporous membrane based on ZIF-7 doped 1,2-bis (triethoxysilyl)ethane for H_2/CO_2 separation. Microporous Mesoporous Mater 2022;331:111674. https://doi.org/10.1016/j.micromeso.2021.111674.

[30] Bachman JE, Smith ZP, Li T, Xu T, Long JR. Enhanced ethylene separation and plasticization resistance in polymer membranes incorporating metal-organic framework nanocrystals. Nat Mater 2016;15. https://doi.org/10.1038/NMAT4621. 845-+.

[31] Zhang H, He D, Niu S, Qi H. Tuning the microstructure of organosilica membranes with improved gas permselectivity via the co-polymerization of 1,2-bis(triethoxysilyl) ethane and 1,2-bis(triethoxysilyl)methane. Int J Hydrog Energy 2021;46:17221–30. https://doi.org/10.1016/j.ijhydene.2021.02.139.

[32] Boroglu MS, Yumru AB. Gas separation performance of 6FDA-DAM-ZIF-11 mixed-matrix membranes for H_2/CH_4 and CO_2/CH_4 separation. Sep Purif Technol 2017;173:269–79. https://doi.org/10.1016/j.seppur.2016.09.037.

[33] Shin JE, Lee SK, Cho YH, Park HB. Effect of PEG-MEA and graphene oxide additives on the performance of Pebax® 1657 mixed matrix membranes for CO_2 separation. J Membr Sci 2019;572:300–8. https://doi.org/10.1016/j.memsci.2018.11.025.

[34] Wang Z, Yuan J, Li R, Zhu H, Duan J, Guo Y, et al. ZIF-301 MOF/6FDA-DAM polyimide mixed-matrix membranes for CO_2/CH_4 separation. Sep Purif Technol 2021;264:118431. https://doi.org/10.1016/j.seppur.2021.118431.

[35] Raza W, Jianhua Y, Wang J, Saulat H, Wang L, Lu J, et al. A selective organosilica membrane for ethyl acetate dehydration by pervaporation. J Appl Polym Sci 2021;138:e50942. https://doi.org/10.1002/app.50942.

[36] Ngamou PHT, Overbeek JP, Kreiter R, van Veen HM, Vente JF, Wienk IM, et al. Plasma-deposited hybrid silica membranes with a controlled retention of organic bridges. J Mater Chem A 2013;1:5567–76. https://doi.org/10.1039/c3ta00120b.

[37] Al-Oweini R, El-Rassy H. Synthesis and characterization by FTIR spectroscopy of silica aerogels prepared using several $Si(OR)_4$ and $R''Si(OR')_3$ precursors. J Mol Struct 2009;919:140–5. https://doi.org/10.1016/j.molstruc.2008.08.025.

[38] Kang C-H, Lin Y-F, Huang Y-S, Tung K-L, Chang K-S, Chen J-T, et al. Synthesis of ZIF-7/chitosan mixed-matrix membranes with improved separation performance of water/ethanol mixtures. J Membr Sci 2013;438:105–11. https://doi.org/10.1016/j.memsci.2013.03.028.

[39] Boffa V, Blank DHA, ten Elshof JE. Hydrothermal stability of microporous silica and niobia-silica membranes. J Membr Sci 2008;319:256–63. https://doi.org/10.1016/j.memsci.2008.03.042.

[40] Yoshioka T, Nakanishi E, Tsuru T, Asaeda M. Experimental studies of gas permeation through microporous silica membranes. AIChE J 2001;47:2052–63. https://doi.org/10.1002/aic.690470916.

[41] Xu R, Liu Q, Ren X, Lin P, Zhong J. Tuning the pore structures of organosilica membranes for enhanced desalination performance via the control of calcination temperatures. Membranes 2020;10:392. https://doi.org/10.3390/membranes10120392.

[42] Meng L, Kanezashi M, Wang J, Tsuru T. Permeation properties of BTESE-TEOS organosilica membranes and application to O_2/SO_2 gas separation. J Membr Sci 2015;496:211–8. https://doi.org/10.1016/j.memsci.2015.08.066.

[43] Chen W-H, Chen C-Y. Water gas shift reaction for hydrogen production and carbon dioxide capture: a review. Appl Energy 2020;258:114078. https://doi.org/10.1016/j.apenergy.2019.114078.

[44] Yang T, Xiao Y, Chung T-S. Poly-/metal-benzimidazole nano-composite membranes for hydrogen purification. Energy Environ Sci 2011;4:4171–80. https://doi.org/10.1039/c1ee01324f.

[45] Park S, Cho KY, Jeong H-K. Polyimide/ZIF-7 mixed-matrix membranes: understanding the*in situ*confined formation of the ZIF-7 phases inside a polymer and their effects on gas separations. J Mater Chem A 2020;8:11210–7. https://doi.org/10.1039/d0ta02761h.

[46] Mei X, Yang S, Lu P, Zhang Y, Zhang J. Improving the selectivity of ZIF-8/polysulfone-mixed matrix membranes by polydopamine modification for H_2/CO_2Separation. Front Chem 2020;8:528. https://doi.org/10.3389/fchem.2020.00528.

[47] Al-Maythalony BA, Alloush AM, Faizan M, Dafallah H, Elgzoly MAA, Seliman AAA, et al. Tuning the interplay between selectivity and permeability of ZIF-7 mixed matrix membranes. ACS Appl Mater Interfaces 2017;9:33401–7. https://doi.org/10.1021/acsami.6b15803.

[48] Zhao Y, Zhou C, Kong C, Chen L. Ultrathin reduced graphene oxide/organosilica hybrid membrane for gas separation. JACS Au 2021;1:328–35. https://doi.org/10.1021/jacsau.0c00073.

[49] Ren X, Kanezashi M, Guo M, Xu R, Zhong J, Tsuru T. Multiple amine-contained POSS-functionalized organosilica membranes for gas separation. Membranes 2021;11:194. https://doi.org/10.3390/membranes11030194.